RAPID COMMUNICATION

Effects of V/III ratio on *a*-plane GaN epilayers with an InGaN interlayer*

Wang Jian-Xia(王建霞)†, Wang Lian-Shan(汪连山)‡, Yang Shao-Yan(杨少延)§, Li Hui-Jie(李辉杰)
Zhao Gui-Juan(赵桂娟), Zhang Heng(张 恒), Wei Hong-Yuan(魏鸿源),
Jiao Chun-Mei(焦春美), Zhu Qin-Sheng(朱勤生), and Wang Zhan-Guo(王占国)

Key Laboratory of Semiconductor Materials Science, Beijing Key Laboratory of Low Dimensional Semiconductor Materials and Devices, Institute of Semiconductors, Chinese Academy of Sciences, Beijing 100083, *China*

(Received 18 July 2013; revised manuscript received 13 August 2013; published online 10 December 2013)

The effects of V/III growth flux ratio on *a*-plane GaN films grown on *r*-plane sapphire substrates with an InGaN interlayer are investigated. The surface morphology, crystalline quality, strain states, and density of basal stacking faults were found to depend heavily upon the V/III ratio. With decreasing V/III ratio, the surface morphology and crystal quality first improved and then deteriorated, and the density of the basal-plane stacking faults also first decreased and then increased. The optimal V/III ratio growth condition for the best surface morphology and crystalline quality and the smallest basal-plane stacking fault density of *a*-GaN films are found. We also found that the formation of basal-plane stacking faults is an effective way to release strain.

Keywords: V/III ratio, *a*-plane GaN, InGaN interlayer, metalorganic chemical vapor deposition

PACS: 68.37.Ps, 68.55.A–, 78.55.Cr, 81.15.Gh **DOI:** 10.1088/1674-1056/23/2/026801

1. Introduction

Currently, III-nitrides have been widely used in the fields of optoelectronics and microelectronics, such as blue/green light-emitting diodes (LEDs), laser diodes, and solar cells. Most of the commercial GaN-based devices are grown along the polar *c* axis. However, the efficiency of these devices is greatly limited by the existence of built-in electric fields along the *c*-axis direction, which are caused by spontaneous and piezoelectric polarizations in wurtzite nitride materials.[1] The non-polar *a*-plane GaN (*a*-GaN) films, which can be free of the built-in electric fields, are thus expected to have a distinct advantage over conventional *c*-plane films in the fabrication of high-efficiency LEDs. However, the internal quantum efficiency of LEDs based on non-polar GaN grown on foreign substrates (such as *r*-sapphire) is still lower than that of films based on *c*-plane sapphire substrates. The main reasons lie in two characteristics of the surface morphology — triangular/pentagonal surface pits[2,3] and a high density of structural defects (including threading dislocations (TDs) and basal-plane stacking faults (BSFs) bounded by partial dislocations (PDs)[4–7] that arise from the planar anisotropic nature of the growing surface). Hence, the improvement of the crystal quality of non-polar nitrides still needs more effort. In this paper, we report how the V/III ratio of *a*-GaN growth was optimized.

Due to the anisotropic nature of the growing surface, the vertical and lateral growth rates of non-polar *a*-GaN surfaces depend heavily on the V/III ratio and the growth pressure: high V/III ratio and high pressure promote predominantly vertical growth and result in three-dimensional (3D) island growth, while low V/III ratio and low reactor pressure give rise to predominantly lateral growth.[8,9] We grew *a*-GaN films under low reactor pressure with different V/III ratios and systematically investigated the films' surface properties, crystalline quality, and strain states, as well as the density of basal-plane stacking faults. A key InGaN interlayer, which was proven in our previous work to improve the surface morphology and crystal quality,[10,11] was deposited on the substrate before the deposition of *a*-GaN film. Upon testing the samples, it was found that the characteristics of the *a*-GaN films change non-monotonically with changing V/III ratio.

2. Experiments

All the a-plane $(11\bar{2}0)$ GaN films were grown on *r*-plane $(1\bar{1}02)$ sapphire substrates in a specially crafted horizontal low-pressure metal–organic chemical vapor deposition (MOCVD) system using trimethylgallium (TMG), trimethylindium (TMI), and ammonia as precursors. Prior to

*Project supported by the National Natural Science Foundation of China (Grant Nos. 91233111, 61274041, 11275228, 61006004, and 61076001), the Special Funds for Major State Basic Research Project (973 Program) of China (Grant No. 2012CB619305), the 863 High Technology R & D Program of China (Grant No. 2011AA03A101) and the Special Fund for LED Industrial Development of Guangdong Province of China (Grant No. 2012A080302003).

†Corresponding author. E-mail: ls-wang@semi.ac.cn

‡Corresponding author. E-mail: ls-shan@semi.ac.cn

§Corresponding author. E-mail: sh-yyang@semi.ac.cn

© 2014 Chinese Physical Society and IOP Publishing Ltd

the epitaxial growth, the *r*-plane sapphire substrates were nitridized for 3 min under NH_3 with a flow of 3 SLM (standard liter per minute). Then, the thin InGaN interlayer was deposited on the *r*-plane sapphire substrate at 750 °C and 200 Torr (1 Torr = 1.33322×10^2 Pa), the flow rates of the TMG, TMI, and ammonia were 10 μmol/min, 20 μmol/min, and 3 SLM, respectively; the InGaN thickness was approximately 115 nm and the In fraction was about 41%. After which, a conventional LT-GaN buffer layer of ∼ 30-nm thickness was deposited above the InGaN layer with flow rates of TMG and NH_3 of 35.7 μmol/min and 3 SLM, respectively, and the V/III ratio was approximately 4500. Subsequently, the LT-GaN/InGaN/*r*-sapphire structures were annealed *in-situ* at 1100 °C for 3 min, obtaining reticular stripe templates, which improve compliance. Finally, a high temperature GaN regrowth under different V/III ratio was performed on the template at 1100 °C and 50 Torr, the flow rate of TMG during the GaN regrowth was fixed at 35.7 μmol/min. Different V/III ratios from 500 to 2000, yielding samples which are successively named samples A–F, were achieved by modulating the flow rate of NH_3 from 0.4 SLM to 1.6 SLM. The growth parameters of the samples are all the same except for the NH_3 flow of the *a*-GaN epilayers. The total flow was constant. The growth time was fixed at 1 hour. Details of the samples are shown in the Table 1.

Table 1. Growth parameters and BSF density results of samples A–F.

Sample No.	NH_3 flow/SLM	V/III ratio	LCL/nm	BSF density/10^5 cm^{-1}
A	0.4	500	22.90	4.85
B	0.6	750	27.68	4.01
C	0.8	1000	27.45	4.05
D	1.0	1250	28.72	3.86
E	1.2	1500	18.10	6.14
F	1.6	2000	17.46	6.36

The surface morphology of these *a*-GaN films were characterized by atomic force microscopy (AFM), and the tapping mode was employed. The structural properties of the films were investigated by high-resolution X-ray diffraction (HRXRD). The HRXRD data were obtained at 1W1A, Beijing Synchrotron Radiation Facility (BSRF). The radiation energy of the light was 8.05 keV, the spot size was 0.7 mm×0.4 mm ($H\times V$), and the wavelength used was 1.5493 Å; a Huber five-circle diffractometer was used.

3. Results and discussion

Figure 1(a) shows the schematic growth model of the *a*-GaN growth; figure 1(b) shows the SEM micrograph of the LT-GaN/InGaN/sapphire template after *in-situ* high temperature annealing, which results in reticular stripes along the [0001] orientation. The template with reticular stripes is able to elastically accommodate any lattice mismatch between the substrate and the film, and then release the strain in the *a*-GaN epilayer. The remarkable improvement of the surface morphology and crystal quality due to the InGaN interlayer has been proved.[11]

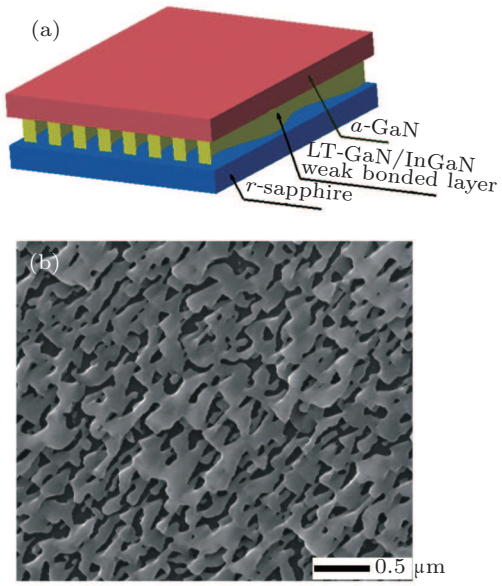


Fig. 1. (color online) (a) Schematic growth model of *a*-GaN/LT-GaN/InGaN/*r*-sapphire structure; panel (b) SEM micrograph of LT-GaN/InGaN/sapphire after *in-situ* high temperature annealing.

Aiming to obtain the information of the crystalline quality of the samples, a HRXRD analysis of the $(11\bar{2}0)$ ω scans as a function of V/III ratio was performed. Figure 2 shows the V/III ratio dependence of the full widths at half maximum (FWHM) of the rocking curves for $\phi = 0°$, 30°, 60°, and 90°, respectively. $\phi = 0°$ is the *c* [0001] axis and $\phi = 90°$ corresponds to the *m* $[1\bar{1}00]$ axis. High-V/III-ratio samples E and F exhibit large FWHMs; for lower V/III ratios (samples A–D), the FWHMs were much smaller. But with decreasing V/III ratio, the FWHM values along the four axes all first decrease and then increase in a roughly similar progression. The lower FWHM values of rocking curves indicate a lower density of defects. Sample D, having the smallest FWHM values, shows the best crystalline quality. This evidence of the dependence of crystal quality on the V/III ratio is quite consistent with the surface morphology analysis by AFM, shown in Fig. 3.

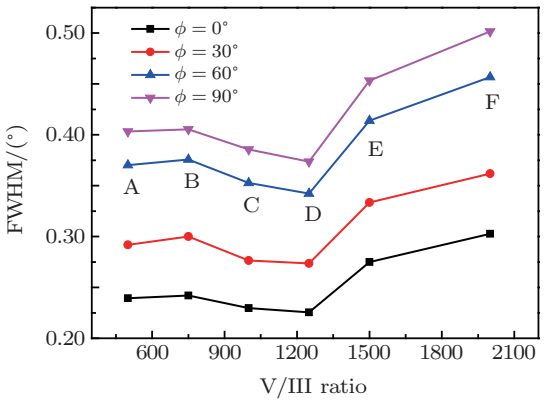


Fig. 2. (color online) Full width at half maximum values as functions of the V/III ratio.

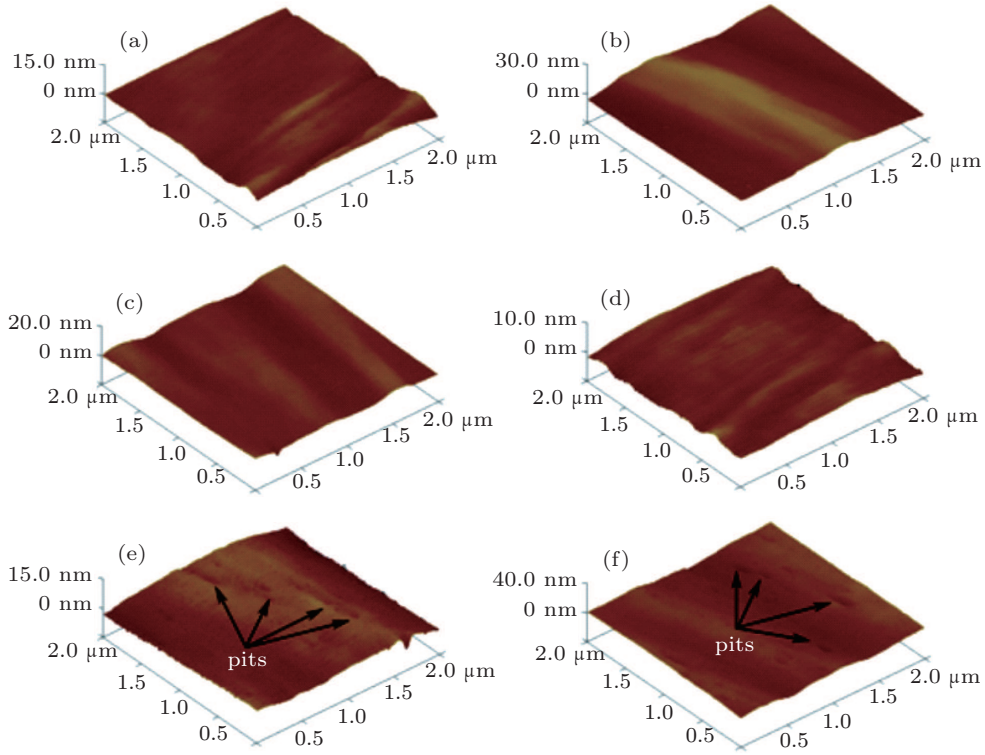


Fig. 3. (color online) AFM images of the six samples. Panels (a)–(f) correspond to samples A–F.

The 2 μm×2 μm AFM images of the samples are shown in Fig. 3. At a relatively high V/III ratio (1500, 2000), samples E and F present small surface pits, which originate from island growth and coalescence during the initial growth of the *a*-GaN. With lower V/III ratios, samples A–D exhibit pit-free but striped surfaces. A lower V/III ratio enhances 2D growth as well as eliminates pits. These results correspond with the findings of others[12–14] who reported that surface morphology can be improved by growing *a*-GaN with a low V/III ratio and a low reactor pressure, conditions which also facilitate 2D growth. The values of root mean square (RMS) roughness of the surfaces for samples A–F are 0.732, 2.99, 1.12, 0.501, 1.4, and 2.4 nm, respectively. The RMS roughness changes non-monotonously with decreasing V/III ratio, mainly decreasing and then increasing. Sample D (V/III = 1250) presents the smallest RMS roughness. The pitted surface morphology of samples E and F can be attributed to the fact that an excess of hydrogen atoms, inherent in the high V/III ratio, facilitates the surface dissociation rate and damages the surface morphology.[15] With lower V/III ratios, the pits were completely eliminated, due to the reduction of hydrogen atoms, although with some stripes along the [0001] direction. The possible reason for the stripes forming is the faster growth rate along the *c* direction than along the *m* direction. Although the low V/III ratio benefits 2D growth, some Ga atoms do not react, due to an insufficiency of N atoms, thereby causing a wavy surface. The AFM results indicate that the surface morphology of the as-grown *a*-GaN film is greatly affected by the V/III ratio. The same reasons apply in explaining the dependence of crystal quality on the V/III ratio. In this study, the surface morphology and crystalline quality of *a*-GaN films presented the same properties with decreasing V/III ratio: first improving and then deteriorating. It is crucial to grow *a*-GaN under an appropriate V/III ratio in order to achieve a fine surface morphology and better crystal quality. The optimal V/III ratio (1250) for the best surface morphology and crystal quality was obtained. The *a*-GaN crystal quality can still be improved further by optimizing other conditions of the growth process.

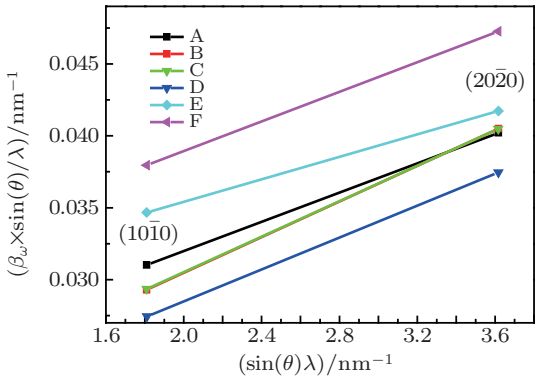


Fig. 4. (color online) Modified WH plots. The straight lines are the linear fits to the (10$\bar{1}$0) and (20$\bar{2}$0) data-points of each sample.

McLaurin *et al.*[16] proposed a model treating BSFs as boundaries between incoherently scattering domains, and determined the lateral coherence length (LCL) of *m*-GaN film through a modified Williamson–Hall (WH) analysis. The

same concept was applied here to determine the c-axis LCL and estimate the BSF density in the a-GaN films. Because a-plane $(11\bar{2}0)$ diffraction is insensitive to the presence of BSFs, a modified WH analysis was carried out with the inclined $(10\bar{1}0)$ and $(20\bar{2}0)$ reflections in a skew symmetric geometry with the X-ray rocking along the c axis (Fig. 4).[17] The growth parameters, reduced LCL along c axis, and the BSF density in a-GaN film are also shown in Table 1. We found that the BSF density also roughly first decreases and then increases; the lowest BSF density was also obtained in sample D (V/III = 1250). Such a dependence of BSF density on the V/III ratio is also very consistent with the FWHM values of XRC shown in Fig. 2 and the surface morphology analysis by AFM shown in Fig. 3. In addition, samples E and F with some pits have the highest BSF density, so it can be concluded that the pits are related to the BSF density.

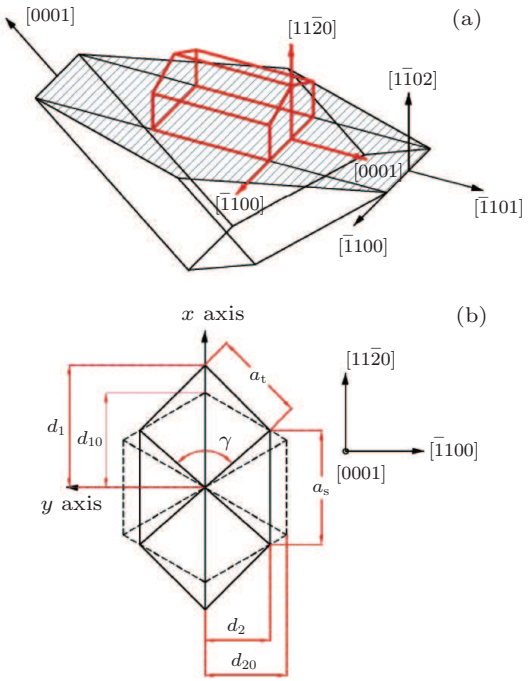


Fig. 5. (color online) (a) Schematic illustration of the epitaxial relationship between a-GaN and the r-plane sapphire. (b) Distortion of the basal hexagon of the GaN unit cell under anisotropic strain for a-GaN film (the undistorted hexagon is shown by the dashed line). Here $d_1 = 2d_{11\bar{2}0}$, $d_2 = d_{1\bar{1}00}$, a_s is the sidewall lattice parameter, a_t is the top lattice parameter, and γ is the distortion angle.[18]

Masihhur R. Laskar reported a method of determining the lattice parameters and strain values of a-plane nitrides,[19] which was used here to estimate the lattice constants and strain values ε_{xx}, ε_{yy}, and ε_{zz} along the $[11\bar{2}0]$, $[10\bar{1}0]$, [0001] orientations, respectively. The 2θ values of the six reflections $(11\bar{2}0)$, $(10\bar{1}0)$, $(20\bar{2}0)$, $(10\bar{1}1)$, $(10\bar{1}2)$, and $(11\bar{2}2)$ for all samples were measured (but are not given here).

The epitaxial relationship between a-GaN and r-sapphire is shown schematically in Fig. 5(a). For simplicity, we define the x, y, and z axes parallel to the $[11\bar{2}0]$, $[10\bar{1}0]$, [0001] orientations of a-GaN, respectively. The epitaxial relationship between a-GaN and r-sapphire is given by

$$y \,\|\, [\bar{1}100]_{Al_2O_3} \,\|\, [11\bar{2}0]_{GaN}, \quad z \,\|\, [\bar{1}101]_{Al_2O_3} \,\|\, [0001]_{GaN}.$$

The strain in the basal plane is not isotropic. Since the basal plane of the GaN is distorted, the hexagonal symmetry of the unit cell is broken, and the GaN turns into an orthorhombic crystal with three independent lattice parameters a_s, c, and γ (Fig. 5(b)).

For an a-plane epilayer, the strain values in each direction can be expressed by

$$\varepsilon_{xx} = \frac{(d_1 - d_{10})}{d_{10}}, \quad \varepsilon_{yy} = \frac{(d_2 - d_{20})}{d_{20}}, \quad \varepsilon_{zz} = \frac{(c - c_0)}{c_0},$$

where $d_1 = 2d_{11\bar{2}0} = (2a_t \sin\gamma)/\sqrt{2(1-\cos\gamma)}$, $d_2 = d_{1\bar{1}00} = (a\sin\gamma)/\sqrt{2(1+\cos\gamma)}$ for the distorted epilayers, whereas d_{10} and d_{20} are the corresponding values for the fully relaxed (undistorted) epilayer as indicated schematically in Fig. 5(b). The calculated lattice constants and strain values for the samples are shown in Table 2. We can see that the strain ε_{xx} along the x orientation is tensile, and ε_{yy} and ε_{zz} are compressive for all the samples, which is consistent with theoretical predictions and experiments conducted by other researchers.[20] It can also be seen that nearly all the strain along the three orientations decreases with increasing V/III ratio. Especially for samples E and F, the strains ε_{yy} and ε_{zz} are much less than those for the other samples. Some groups reported that the strain relaxation in non-polar a-GaN can be attributed to the formation of the BSFs.[21,22] So for samples E and F, with high density BSFs, the strain is greatly released.

Table 2. Sidewall lattice parameters a_s, top lattice parameters a_t, c, angle of distortion of the basal plane γ of a set of a-GaN epilayers, and the strains ε_{xx}, ε_{yy}, and ε_{zz}, along the $[11\bar{2}0]$, $[10\bar{1}0]$, [0001] orientations obtained from HRXRD are listed.

Sample	a_t	c	a_s	γ	ε_{xx}	ε_{yy}	ε_{zz}
A	3.1866	5.1798	3.1947839	119.831	0.0018137	–0.00160	–0.00101
B	3.1872	5.1806	3.1947842	119.842	0.0018138	–0.00138	–0.00085
C	3.1878	5.1804	3.1947856	119.856	0.0018142	–0.00108	–0.00090
D	3.1871	5.1809	3.1945606	119.844	0.0017437	–0.00142	–0.00078
E	3.1888	5.1811	3.1941153	119.889	0.0016041	–0.00063	–0.00076
F	3.1897	5.1813	3.1940431	119.911	0.0015814	–0.00022	–0.00071

4. Conclusion

In summary, a strong dependence of surface morphology properties, crystal quality, BSF density, and strain of the *a*-GaN films on V/III ratio has been demonstrated. Unlike other reported studies, we found that with decreasing V/III ratio, crystal quality first improved and then deteriorated, the BSFs density and the RMS of the surface of the samples also roughly first decreased and then increased. The sample D (V/III = 1250) possesses the best surface morphology and crystal quality, and the smallest BSF density. The strain of samples E and F, which possess a high density of BSFs, is largely released compared to samples A–D, from which it can be concluded that the formation of the BSFs is very effective to release the strain in *a*-GaN epilayer.

Acknowledgments

A portion of this work is based on the data obtained at 1W1A, Beijing Synchrotron Radiation Facility (BSRF). The authors gratefully acknowledge the assistance of the staff of the Diffuse X-ray Scattering Station during the experiments.

References

[1] Bermardini F, Fiorentini V and Vanderbilt D 1997 *Phys. Rev. B* **56** R10024
[2] Sun Q, Yerino C D, Ko T S, Cho Y S, Lee I H, Han J and Coltrin M E 2008 *J. Appl. Phys.* **104** 093523
[3] Hollander J L, Kappers M J, McAleese C and Humphreys C J 2008 *Appl. Phys. Lett.* **92** 101104
[4] Zakharov D N, Liliental-weber Z, Wagner B, Reitmeier Z J, Preble E A and Davis R F 2005 *Phys. Rev. B* **71** 235334
[5] Liu R, Bell A, Ponce F A, Chen C Q, Yang J W and Khan M A 2005 *Appl. Phys. Lett.* **86** 021908
[6] Gühne T, Bougrioua Z, Vennéguès P, Leroux M and Albrecht M 2007 *J. Appl. Phys.* **101** 113101
[7] Wu Z H, Fischer A M, Ponce F A, Bastek B, Christen J, Wernicke T, Weyers M and Kneissl M 2008 *Appl. Phys. Lett.* **92** 171904
[8] Sun Q, Kong B H, Yerino C D, Ko T S, Leung B, Cho H K and Han J 2009 *J. Appl. Phys.* **106** 123519
[9] Tian Y, Dai J N, Xiong H, Zheng G, Ryu M, Fang Y Y and Chen C Q 2012 *Chin. Phys. Lett* **29** 088101
[10] Xu X Q, Guo Y, Liu X L, Liu J M and Song H P 2011 *Cryst. Eng. Comm.* **13** 1580
[11] Li Z W, Wei H Y, Xu X Q, Zhao G J, Liu X L, Yang S Y, Zhu Q S and Wang Z G 2012 *J. Cryst. Growth* **348** 10
[12] Ni X, Fu Y, Moon Y T, Biyikli N and Morko H 2006 *J. Cryst. Growth* **290** 166
[13] Ko T S, Wang T C, Gao T C, Chen H G, Huang G S, Lu T C, Kuo H C and Wang S C 2007 *J. Cryst. Growth* **300** 308
[14] Miyagawa R, Narukawa M, Ma B, Miyake H and Hiramatsu K 2008 *J. Cryst. Growth* **310** 4979
[15] Xie Z L, Li Y, Liu B, Zhang R, Xiu X Q, Chen P and Zheng Y L 2011 *Chin. Phys. B* **20** 106801
[16] Mclaurin M B, Hirai A, Young E, Wu F and Speck J S 2008 *Jpn. J. Appl. Phys.* **47** 5429
[17] Sun Q, Ko T S, Yerino C D, Zhang Y, Lee I H, Han J, Lu T C, Kuo H C and Wang S C 2009 *Jpn. J. Appl. Phys.* **48** 071002
[18] Zhao G J, Yang S Y, Liu G P, Liu C B, Sang L, Gu C Y, Liu X L, Wei H Y, Zhu Q S and Wang Z G 2013 *Chin. Phys. Lett.* **30** 098102
[19] Laskar M R, Ganguli T, Rahman A A, Mukherjee A, Hatui N, Gokhale M R and Bhattacharya A 2011 *J. Appl. Phys.* **109** 013107
[20] Ghosh S, Misra P and Grahn H T 2005 *J. Appl. Phys.* **98** 026105
[21] Kong B H, Cho H K, Song K M and Yoon D H 2010 *J. Cryst. Growth* **313** 8
[22] Liu Z Y, Xu S R, Zhang J C, Xue J S, Xue X Y, Niu M T and Hao Y 2012 *J. Cryst. Growth* **343** 122